European Journal of Nuclear Medicine and Molecular Imaging (2019) 46:1733–1744
https://doi.org/10.1007/s00259-019-04318-3

ORIGINAL ARTICLE

Diffusion-weighted MRI and ^{18}F-FDG PET correlation with immunity in early radiotherapy response in BNL hepatocellular carcinoma mouse model: timeline validation

Yi-Hsiu Chung[1] · Ching-Fang Yu[2,3] · Shao-Chieh Chiu[1] · Han Chiu[1] · Shin-Ting Hsu[1] · Ching-Rong Wu[2,3] · Chung-Lin Yang[3,4] · Ji-Hong Hong[2,3,4] · Tzu-Chen Yen[1,5] · Fang-Hsin Chen[2,3,4]

Received: 9 December 2018 / Accepted: 25 March 2019 / Published online: 24 May 2019

Abstract

Purpose Imaging probes/biomarkers that are correlated with molecular or microenvironmental alterations in tumors have been used not only in diagnosing cancer but also in assessing the efficacy of cancer treatment. We evaluated the early response of hepatocellular carcinoma (HCC) to radiation treatment using T2-weighted magnetic resonance imaging (MRI), diffusion-weighted (DW) MRI, and ^{18}F-fluorodeoxyglucose (^{18}F-FDG) positron emission tomography (PET).

Methods Orthotopic HCC tumors were established in the right liver lobe of Balb/c mice. Mice were longitudinally scanned using T2-weighted/DW MRI and ^{18}F-FDG PET 1 day before and on days 1, 3, 6, 9 and 13 after irradiation with 15 Gy to the right liver lobe to determine tumor size, apparent diffusion coefficient (ADC) value, and maximum standardized uptake value. Immunohistochemical (IHC) staining was performed to validate the tumor microenvironment.

Results Irradiation markedly retarded tumor growth in the orthotopic HCC model and led to increaes in ADC values as early as on day 1 after irradiation. Irradiation also resulted in increases in ^{18}F-FDG uptake on day 1 that were sustained until the end of the observation period. IHC staining revealed a decrease in the number of proliferative cells and a continuous macrophage influx into irradiated tumors, which dramatically altered the tumor microenvironment. Lastly, in vitro coculture of HCC cells and macrophages led to interaction between the cells and enhanced the cellular uptake of ^{18}F-FDG.

Conclusion ADC values and ^{18}F-FDG uptake measured using DW MRI and ^{18}F-FDG PET serve as potential biomarkers for early assessment of HCC tumor responses to radiation therapy.

Keywords Hepatocellular carcinoma · Radiation therapy · ^{18}F-FDG · Diffusion-weighted MRI · Inflammation

Yi-Hsiu Chung and Ching-Fang Yu contributed equally to this work. Tzu-Chen Yen and Fang-Hsin Chen are corresponding authors.

Electronic supplementary material The online version of this article (https://doi.org/10.1007/s00259-019-04318-3) contains supplementary material, which is available to authorized users.

✉ Tzu-Chen Yen
yentc1110@gmail.com

✉ Fang-Hsin Chen
fanghsinchen@mail.cgu.edu.tw

[1] Center for Advanced Molecular Imaging and Translation (CAMIT), Chang Gung Memorial Hospital Linkou Branch, Taoyuan 333, Taiwan

[2] Department of Radiation Oncology, Chang Gung Memorial Hospital Linkou Branch, Taoyuan, Taiwan

[3] Radiation Biology Research Center, Institute for Radiological Research, Chang Gung University/Chang Gung Memorial Hospital, Linkou Branch, Taoyuan, Taiwan

[4] Department of Medical Imaging and Radiological Sciences, Chang Gung University, Taoyuan City, Taiwan

[5] Department of Nuclear Medicine, Chang Gung Memorial Hospital Linkou Branch, Taoyuan 333, Taiwan

Introduction

Hepatocellular carcinoma (HCC)—the predominant type of primary liver cancer—is the sixth most common cancer and the third leading cause of cancer deaths worldwide [1, 2]. In palliative treatment of HCC, external-beam radiation therapy has played only a limited role because radiation induces other liver diseases [3]. However, with the advanced technologies now available that can precisely deliver sufficient radiation doses to tumors sparing surrounding normal liver tissue, radiotherapy is receiving increased attention for the treatment of HCC patients [4]. According to radiation therapy guidelines based on the Response Evaluation Criteria in Solid Tumors, tumor re-evaluation every 6–8 weeks during treatment is considered an appropriate evaluation frequency [5], and patients are typically enrolled for imaging examinations with, for example, ultrasonography and computed tomography (CT), at 5–8 weeks after completion of the entire treatment course. However, in certain patients the tumor may not respond well to radiation treatment, and this might be associated with a poor prognosis after completion of treatment. Therefore, patients could benefit from timely adjustment of the treatment regimen if the tumor response could be assessed early; however, suitable modalities for early assessment of tumor response are still lacking.

Functional imaging plays a crucial role in healthcare. Unlike CT and conventional magnetic resonance imaging (MRI) scans, which provide primarily anatomic information, molecular radiotracers used in positron emission tomography (PET) and in diffusion-weighted (DW) MRI and dynamic contrast-enhanced (DCE) MRI provide various types of information that can reveal alterations in the tumor microenvironment following radiation therapy [1, 6, 7]. ^{18}F-Fluorodeoxyglucose (^{18}F-FDG) uptake has been shown to be dramaticallly increased in inflammatory lesions of tumors exposed to radiation in which NF-κB upregulation mediates antiapoptotic functions by inducing pro-inflammatory genes [8, 9]. However, the timeline of the radiation-induced inflammatory response remains poorly understood. Thus, the timing of clinical PET after radiation therapy is carefully selected to avoid inflammation-related problems [10]. Conversely, MRI has been used in patients with small HCC after stereotactic ablative body irradiation therapy, and with gadoxetic acid contrast enhancement, the threshold dose for loss of liver tissue can be predicted [11]. Moreover, MRI yields more useful information than ultrasound imaging for monitoring the growth of orthotopic tumors and for accurately estimating the tumor doubling time [12]. Furthermore, DW MRI provides apparent diffusion coefficient (ADC) values, which correlate with cell density and serve as an indicator of alterations in the tumor microenvironment [13].

In the study reported here, we analyzed early tumor responses following radiation therapy using noninvasive PET and MRI to validate treatment accuracy. Orthotopic tumor models are superior to subcutaneous tumor models in mimicking the genuine tumor microenvironment that supports tumor progression, but the major drawback of orthotopic models is that tumor volume and the microenvironment cannot be measured and characterized directly unless the animals are killed. However, by using noninvasive multi-imaging, spatiotemporal information regarding the tumor microenvironment, including changes even at the molecular level, can be acquired and quantified. Therefore, we sought to identify early alterations in the tumor microenvironment in a preclinical orthotopic HCC model following radiation therapy using non-invasive T2-weighted/DW MRI and ^{18}F-FDG PET sequentially.

Materials and methods

Experimental design

In vivo imaging and ex vivo studies, and in vitro measurements of ^{18}F-FDG cellular uptake were performed to characterize the biological alterations occurring in irradiated tumors at various time-points after treatment. All mice were screened using bioluminescence imaging to determine the success of tumor development before irradiation. T2-weighted MRI was performed in tumor-bearing mice 10 days after tumor injection to determine tumor sizes [14]. Mice bearing tumors of a suitable size were randomly assigned to a no-radiation group (non-RT) group and a radiation group (RT). Not all mice were used for each imaging modality, and at least three replications were included on each measurement day, except the last day. The total number of experimental mice undergoing MRI T2/DW was 21 and only half of the mice ($n = 13$) were also examined by sequential FDG PET imaging at selected time-points. The numbers of animals used in imaging studies are shown in Fig. 1. Another independent ex vivo study was performed to validate the results of in vivo imaging. Mice were killed on day 1, 3 or 6 after irradiation, which corresponded to the days selected for imaging studies, and three tumors were collected from the non-RT and RT groups. HCC cells and RAW 264.7 cells were cultured separately in Transwell dishes (1.0 μm PET; Millipore, Burlington, MA) or cocultured in 12-well culture plates, and after irradiation with 2 Gy, were evaluated for ^{18}F-FDG uptake at 3 and 24 h. The experimental flow chart is shown in Fig. 1.

Cell line cultures

The murine HCC cell line BNL 1ME A.7R.1 expressing the firefly luciferase gene was obtained from Professor Chia-Rui Shen, Chung Gung University, and the murine macrophage

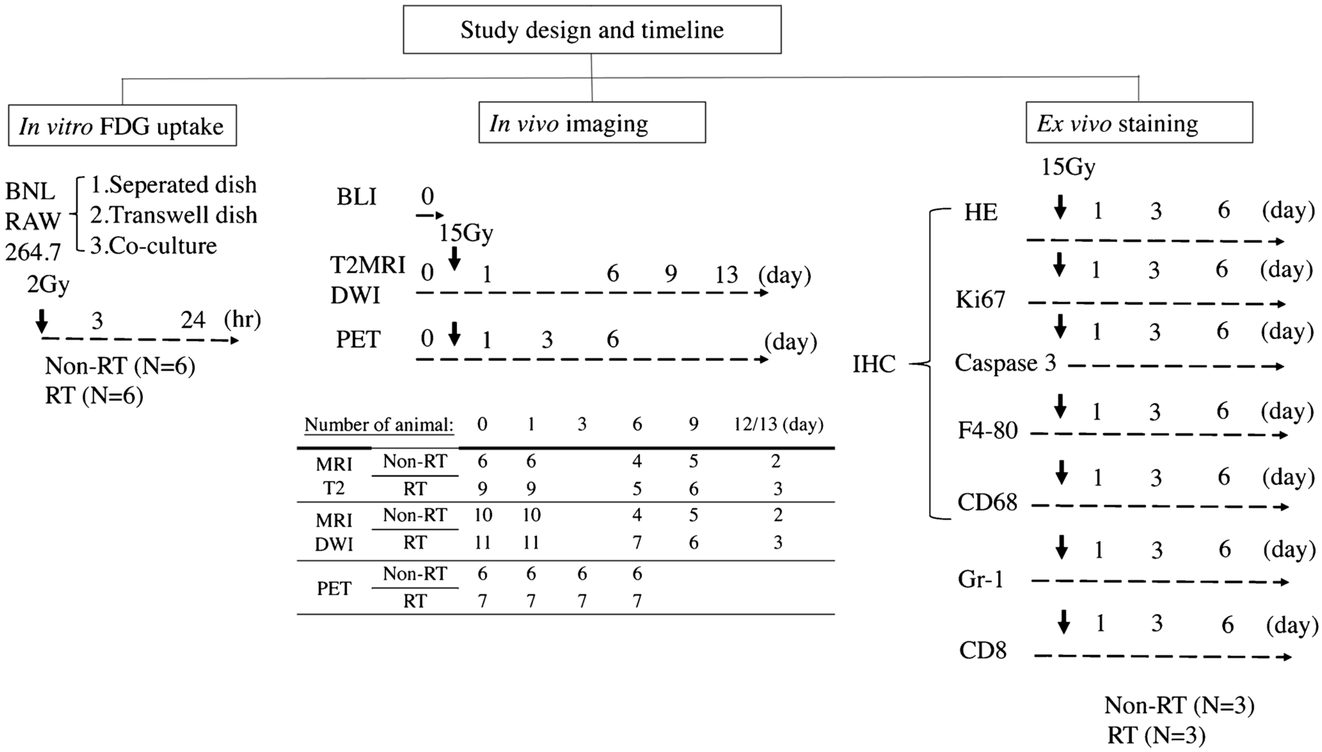

Fig. 1 Flow chart for in vitro culturing, in vivo imaging, and ex vivo validation. For in vitro studies, all experiments were conducted in triplicate and repeated twice. For in vivo and ex vivo studies, the numbers of animals used in imaging and immunohistochemistry experiments are shown. Time-points before and after irradiation selected for each imaging scan are also indicated

cell line RAW 264.7 was purchased from the American Type Culture Collection (ATCC® TIB-71™; ATCC, Manassas, VA). Cells were maintained in Dulbecco's modified Eagle's medium containing 10% fetal bovine serum and 1% penicillin/streptomycin (all reagents from GIBCO, Thermo Fisher Scientific, Inc., Waltham, MA) and incubated at 37 °C in humidified air containing 5% CO_2.

Orthotopic HCC tumor model

Murine HCC BNL cells were orthotopically implanted in the liver of 8-week-old male Balb/c mice. Briefly, after induction of anesthesia with isoflurane and median laparotomy, the surface of the right liver lobe was exposed, and BNL cells (1×10^5 cells suspended in 20 μL of Hanks' balanced salt solution) were injected into the liver subcapsular region using a 30-G needle. The experimental protocols were in accordance with the animal guidelines set out and approved by the Institutional Animal Care and Use Committee of National Tsing Hua University, Taiwan (IACUC 10414).

Animal irradiation

Mice were anesthetized using a 1:1 mixture of ketamine (50 mg/mL) and 1% xylazine (Rompun) and restrained using adhesive tape during irradiation. For partial irradiation to the right liver, the sternum and xiphoid process were used as surface markers to delineate the irradiation field (20 × 10 mm), which covered the region from 10 mm to the right of the sternum and from 10 mm above and 10 mm below the sternum to the xiphoid process. The right liver lobe was irradiated with 15 Gy by 6-MV X-ray beams from a linear accelerator at a dose rate of 6 Gy/min and covered with a 0.5-cm bolus to the skin surface. All animal irradiation and image acquisition protocols were performed in accordance with the animal guidelines set out and approved by the Institutional Animal Care and Use Committee of Chang Gung Memorial Hospital, Taiwan (IACUC 2016010701).

In vivo T2-weighted/DW MRI

A 7-T magnetic resonance scanner (ClinScan; Bruker, Karlsruhe, Germany) was used to monitor tumor responses following radiotherapy. Tumor-bearing mice were secured in the center of the magnet using an acrylic holder and anesthetized with isoflurane (1–2%) during the entire MRI procedure. T2-weighted imaging was first performed to evaluate tumor size according to the difference in T2 relaxation between the orthotopic liver tumor and the surrounding liver tissue. The parameters used for T2-weighted MRI were as follows: turbo spin-echo, TR/TE 2,688/37 ms, slice thickness 1 mm, slice number 14, number of averages 2, echo train length 8, matrix

448 × 226, and flip angle 180°. A total of 14 image datasets were acquired over 2.25 min. Tumor area was manually determined using a region of interest (ROI) tool from transverse T2-weighted MR images. Tumor volume was calculated as tumor ROI × slice thickness. DW MRI sequences were acquired using the following parameters: three gradient directions and two *b* values (0 and 1,000 s/mm^2), TR/TE 3,000/31 ms, matrix size 72 × 128, field of view 25 × 45 mm, number of averages 6, and slice thickness 0.8 mm. ADC values were determined semiautomatically using a threshold (<900 × 10^{-6} mm^2/s) of manually contoured ROIs on ADC maps. All images were analyzed using PMOD version 3.2 image analysis software (PMOD Technologies Ltd., Zurich, Switzerland).

In vivo ^{18}F-FDG PET

Tumor-bearing mice were injected with 8.1 MBq of ^{18}F-FDG via a tail vein and then subjected to a 10-min image acquisition in the prone position after a 60-min uptake period using an Inveon™ system (Siemens Medical Solutions Inc., Malvern, PA). During imaging, mice were anesthetized with 2% isoflurane and placed near the center of the field of view. An infrared heat lamp was used during scanning to prevent hypothermia in the mice. Reconstructed images with a matrix size of 128 × 128 × 159 and a resampling size of 0.39 × 0.39 × 0.80 mm were obtained using the 2D ordered-subsets expectation maximization iterative method. The radioactivity concentrations obtained from microPET images was converted to standardized uptake values (SUV) by multiplying by the individual body weight and dividing by the injected dose. The ROIs were determined semiautomatically using a threshold of 50% of the maximum–minimum SUV range for manually contoured ROIs. ^{18}F-FDG uptake in tumors was expressed as the maximum SUV (SUVmax). All images were analyzed using PMOD version 3.2.

Immunohistochemical analysis

Tumor tissues were embedded in OCT medium (Sakura Finetek, Torrance, CA) and stored at −80 °C. Frozen sections (thickness 10 μm) were fixed with cold 100% methanol (5 min), washed twice with phosphate-buffered saline (PBS), and blocked with PBS containing 1% bovine serum albumin and 0.01% Tween-20 for 1 h at room temperature to minimize nonspecific binding. Sections were next incubated overnight at 4 °C with the following purified antibodies against specific markers: F4/80, CD68 (Bio-Rad, Hercules, CA), Ki67 (Abcam, Cambridge, UK), active-caspase-3 (BD Biosciences, San Jose, CA). Primary antibodies were detected (1 h at room temperature) using fluorescent dye-conjugated secondary antibodies (Invitrogen, Carlsbad, CA). Images were captured on an ImageXpress Micro confocal system (Molecular Devices, San Jose, CA) and analyzed using Image-Pro Plus 6.0.

Real-time PCR

Gene expression was analyzed using a CFX Connect™ real-time PCR system (Bio-Rad, Hercules, CA). Total RNA was isolated using Trizol reagent (Invitrogen) and cDNA was synthesized using an Omniscript reverse transcriptase kit (Qiagen, Hilden, Germany) according to the respective manufacturer's protocol. A quantitative SYBR green PCR assay was performed using a LightCycler® 480 SYBR Green I Master (Roche, Basel, Switzerland) and the paired primers. The fold-change in gene expression in each group was determined as the difference ($\Delta\Delta Ct$) compared to the non-RT group on day 1 after irradiation, where Ct is the threshold value. The sequences of the primers used were as follows: β-actin forward primer, ACCCTAAGGCCAACCGTGAA; β-actin reverse primer, ATGGCGTGAGGGAGAGCATAG; TNF-α forward primer, CACGTCGTAGCA AACCACCA AGTCGA; TNF-α reverse primer, TGGGAGTAGACAAG GTAC AACCC; IL-6 forward primer, AGTTGCCT TCTTGGGACTGA; IL-6 reverse primer, TCCACGAT TTCCCAGAGAAC.

In vitro cell line irradiation and ^{18}F-FDG cellular uptake

BNL HCC cells and RAW 264.7 macrophages were incubated as shown in Fig. 1. Briefly, cells in 12-well culture plates were placed under the collimated beam and subject to a single fractionated irradiation dose of 2 Gy. At 3 and 24 h after irradiation, 1 μCi of ^{18}F-FDG in 0.5 mL of growth medium was added into the culture dishes followed by incubation for for 1 h at 37 °C. Cells were then washed with 1 mL of PBS to remove unabsorbed ^{18}F-FDG, detached by incubating with trypsin-EDTA (GIBCO) for 5 min at 37 °C, and resuspended in growth medium. The total number of cells in each sample was determined using an automatic cell counter (LUNA-FLTM dual fluorescence cell counter; Logos Biosystems, Gyeonggi-do, South Korea). Cell suspensions were further counted for γ-ray emission at 511 keV (Wizard 1480 Gamma Counter; Perkin Elmer, MA). All experiments were performed in triplicate and repeated twice.

Statistical analysis

Statistical analyses were performed using Prism software, version 6 (GraphPad, La Jolla, CA). The data are expressed as means ± standard deviations. ADC values, T2-weighted MRI-derived tumor sizes and the SUVmax of entire tumors were compared between the RT and non-RT groups using Student's *t* test. The statistical significance of differences in macrophage

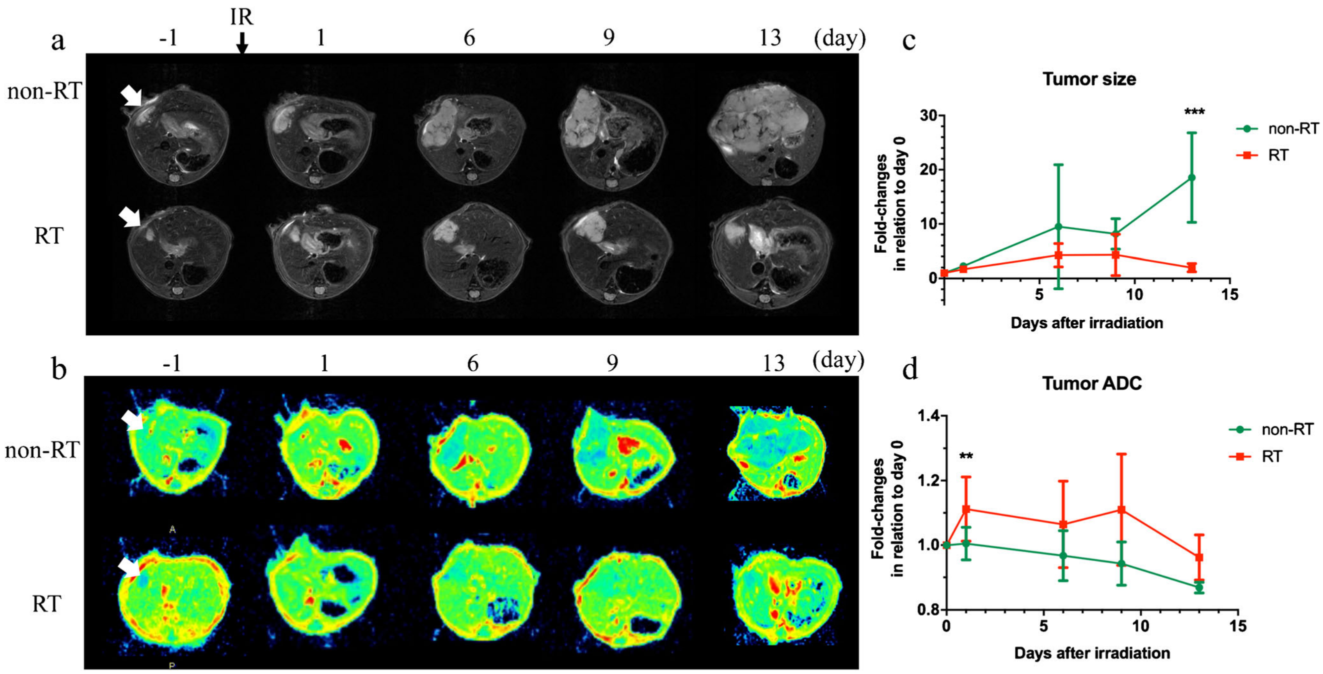

Fig. 2 Effect of radiation therapy on tumor growth and ADC values in orthotopic HCC tumors. **a** Transaxial T2-weighted images show the changes in tumor sizes up to day 13 after irradiation in the non-RT and RT groups. **b** Representative diffusion-weighted (DW) images obtained from corresponding mice. **c** Tumor sizes measured on the indicated days and normalized to those 1 day before irradiation. Tumor growth is significantly delayed in RT group on day 13 (***$P < 0.001$). **d** Changes in ADC values derived from DW images determined on the indicated days and normalized to those 1 day before irradiation. In the RT group the ADC value is significantly increased on day 1 after irradiation (**$P < 0.01$) and thereafter remains higher than in the non-RT group. *White arrows* tumor sites, *IR* irradiation

populations and gene expression was determined by one-way ANOVA. $P \leq 0.05$ was considered statistically significant.

Results

In vivo T2-weighted/DW MRI

MRI was first performed to determine tumor sizes and changes in water diffusion within tumors. Transaxial T2-weighted images from the non-RT and RT groups were examined (Fig. 2a), and tumor sizes on specific days were measured and normalized to those before irradiation (day 0; Fig. 2c). In the non-RT group, tumors developed rapidly, with fold-increases of 2.26 ± 0.65, 9.51 ± 11.4, 8.18 ± 2.81 and 18.56 ± 8.27 on days 1, 6, 9 and 13, respectively. Irradiation markedly inhibited tumor growth: in the RT group fold-increases were 1.70 ± 0.66, 4.25 ± 2.15, 4.31 ± 3.79 and 1.97 ± 0.77 on days 1, 6, 9 and 13, respectively,, with the change being significant on day 13 ($P < 0.001$; Fig. 2c). Our previous DCE MRI study demonstrated spatiotemporal changes in the decrease in K_{trans} during tumor development; this decrease occurs before histological changes and is associated with a worsening tumor response to radiation therapy [15]. These data suggest that early changes in the tumor microenvironment can be detected using functional MRI. Although irradiation did not lead to a substantial change in K_{trans} (data not shown), differential water diffusion velocity in the RT group was identified as early as on day 1 after irradiation by DW MRI. The ADC map converted using the diffusion of water molecules indicated the cell density within tumors (Fig. 2b). ADC values were quantified on the indicated days and normalized to those on day 0 (Fig. 2d). In the non-RT group, tumors showed a continuous decrease in ADC values during growth (fold-changes 1.00 ± 0.05, 0.97 ± 0.08, 0.94 ± 0.07 and 0.87 ± 0.02 on days 1, 6, 9 and 13, respectively). In contrast, in the RT group, ADC values significantly increased on day 1 after irradiation (1.11 ± 0.10, $P < 0.01$), remained elevated on days 6 and 9 (1.06 ± 0.13 and 1.11 ± 0.17), and then decreased on day 13 (0.96 ± 0.07). Thus, a single 15-Gy irradiation of orthotopic HCC tumors caused a prolonged delay in tumor growth and an increase in water diffusion as early as 1 day after radiation therapy, which indicates the differential cell density between non-irradiated and irradiated tumors.

In vivo ^{18}F-FDG PET

To further investigate tumor response following radiation therapy, glucose metabolism in tumors was examined using ^{18}F-FDG PET imaging. ^{18}F-FDG PET and CT images were obtained through whole-body scanning and a fused maximum intensity projection (MIP) was generated (Fig. 3a). The use of

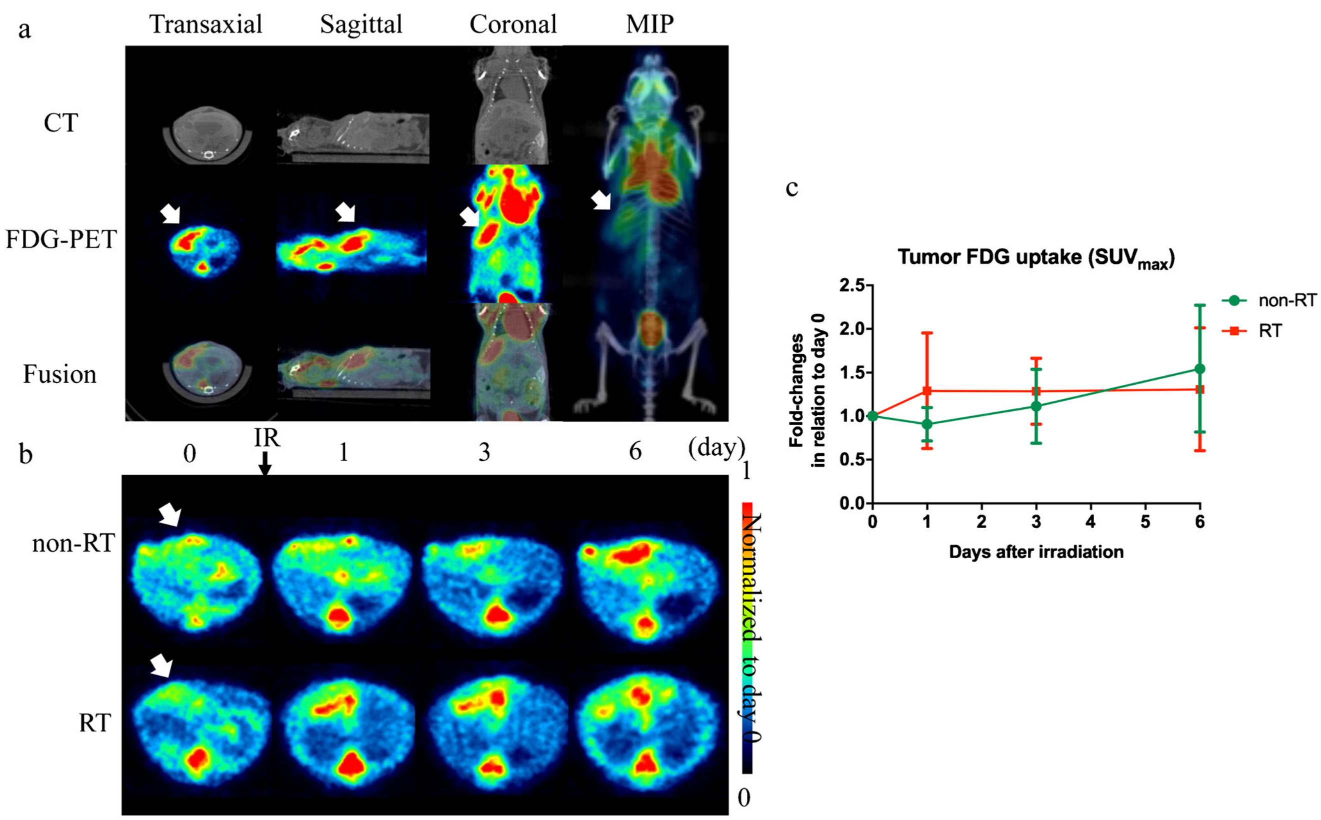

Fig. 3 Effect of radiation therapy on ^{18}F-FDG uptake in orthotopic HCC tumors. **a** Representative coronal, sagittal and transverse ^{18}F-FDG PET, CT and PET/CT images, and the fused maximum intensity projection image. **b** Representative transverse ^{18}F-FDG PET images show uptake in irradiated and non-irradiated tumors. ^{18}F-FDG uptake was evaluated longitudinally on the indicated days. **c** Changes in ^{18}F-FDG uptake measured on the indicated days and normalized to those 1 day before irradiation. *White arrows* tumor sites, *IR* irradiation

anatomic CT images enabled the tumors to be readily identified in the fused images. The temporal pattern of ^{18}F-FDG uptake in the RT and non-RT groups was recorded (Fig. 3b) and the ^{18}F-FDG uptake values obtained were normalized to those before irradiation (day 0; Fig. 3c). ^{18}F-FDG uptake in non-RT tumors gradually increased in accordance with tumor development (fold-changes relative to day 0: 0.91 ± 0.19, 1.11 ± 0.42 and 1.54 ± 0.72 on days 1, 3 and 6, respectively). In contrast, RT triggered a rapid increase in ^{18}F-FDG uptake on day 1 (1.29 ± 0.66) and this level was maintained at 1.29 ± 0.37 and 1.31 ± 0.70 on days 3 and 6, respectively. The ^{18}F-FDG uptake pattern differed between the RT and non-RT groups, although the differences in uptake on the measurement days were not statistically significant.

Immunohistochemical validation of tumor response to irradiation

The MRI and PET results revealed that radiation treatment delayed tumor growth, reduced cell density and increased glucose uptake in the orthotopic HCC model. Hematoxylin and eosin (HE) staining of non-RT and RT tumors ex vivo did not reveal clear differences in cell density (Fig. 4a), but numerous cells harboring small nuclei were detected in RT tumors. Assessment of cell proliferation using the marker Ki67 indicated that about 32–35% of the cells were proliferating in non-RT tumors regardless of the tumor size, but that the percentage of proliferating cells decreased continuously in RT tumors ($28.57 \pm 6.31\%$, $25.53 \pm 5.00\%$ and $17.77 \pm 3.31\%$ on days 1, 3 and 6, respectively; Fig. 4b, c). Moreover, irradiation did not lead to apoptotic cell death, as determined using active caspase-3 staining (data not shown). However, the cellular components in RT tumors showed a dramatic change: macrophage infiltration, identified using markers F4/80 and CD68, was detected as early as on day 1 after irradiation (Fig. 5a, b). Notably, these tumor-infiltrating macrophages harboring small nuclei (identified by DAPI staining) were the same cells as those observed on HE staining, but these macrophages were not the proliferating cells because the Ki67 signal was absent in this population (Fig. 4d). This suggests that macrophage numbers increased over time due to continuous infiltration. These results indicate that the main effects of radiation on HCC tumors during days 1–6 were inhibition of tumor cell proliferation and attraction of macrophage infiltration, which occurred without apoptosis induction.

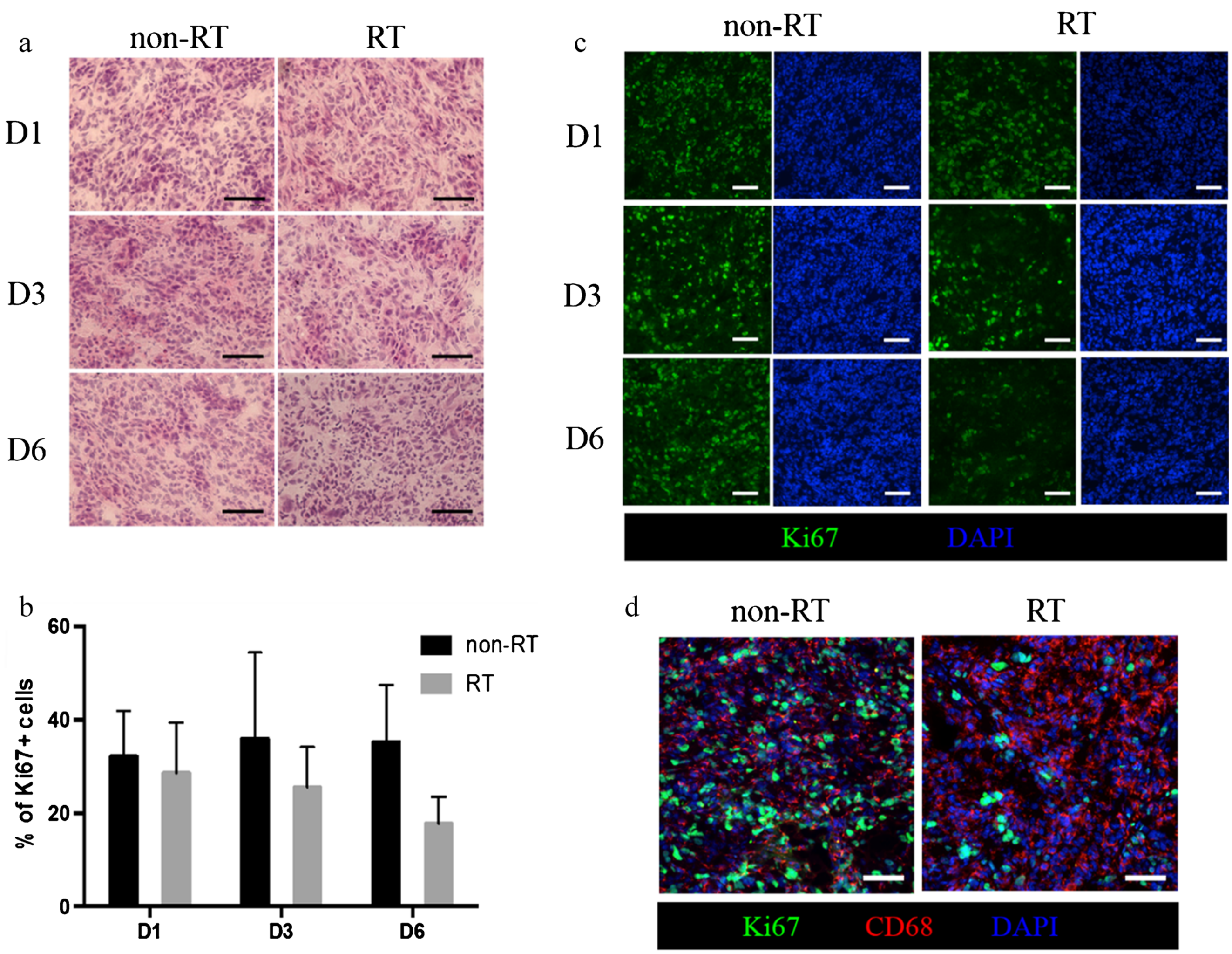

Fig. 4 Radiation therapy reduced HCC proliferation rate in vivo and attracted macrophage infiltration. **a** Representative HE-stained sections of irradiated tumors infiltrated by cells with small nuclei. **b** Representative Ki67-stained and DAPI-stained sections of HCC tumors. (×400, *scale bars* 50 μm). **c** Quantitative comparison of Ki67 staining in non-RT and RT groups (three mice per group). For each tumor, at least eight fields were analyzed. **d** Fluorescent immunohistochemical staining of HCC tumors shows colocalization of CD68 and Ki67 (*red* CD68, *green* Ki67, *blue* DAPI; ×400, *scale bar*50 μm)

Contribution of macrophages to ^{18}F-FDG uptake in tumors

Inflammation has been reported to be associated with increased FDG uptake [8, 9]. To evaluate the mechanism underlying the increased FDG uptake on days 1, 3 and 6 after irradiation (Fig. 3), immunohistochemical (IHC) staining and real-time PCR were performed to assess the immune responses in tumors after irradiation. The F4/80-positive and CD68-positive macrophage populations in IHC images were analyzed based on their pixel numbers in non-RT and RT tumors (Fig. 5a–d). After irradiation, the population of F4/80-positive cells increased gradually: non-RT 2.16 ± 0.21% vs. RT 1.73 ± 0.89% on day 1; non-RT 1.56 ± 0.55% vs. RT 7.14 ± 0.98% on day 3 (P = 0.0245); non-RT 3.11 ± 2.08% vs. RT 11.36 ± 1.13% on day 6 (Fig. 5c). In contrast, CD68-positive cells showed substantial recruitment by day 1 (non-RT 2.01 ± 0.11% vs. RT 5.26 ± 1.18%), and then their population in the tumors remained stable on days 3 and 6 (non-RT 3.82 ± 1.12% vs. RT 7.84 ± 1.22%, P = 0.0061, on day 3; non-RT 2.22 ± 0.65% vs. RT 6.16 ± 0.37% on day 6; Fig. 5d). However, irradiation did not alter Gr-1-positive and CD8-positive cell populations (data not shown), which suggests that neutrophils and T cells likely do not mediate inflammatory responses in tumors or play critical roles in the response of HCC tumors to irradiation. The expression of the inflammatory cytokines, TNF-α and IL-6, in tumors after irradiation was assessed by real-time PCR. TNF-α was significantly induced on day 1 after irradiation (1.66 fold-increase) and increased thereafter on day 6 (3.35 fold-increase; Fig. 5e). IL-6 expression was also increased on day 1 after irradiation (2.41 fold-increase), but declined to basal levels on day 6 (Fig. 5f). These results show that

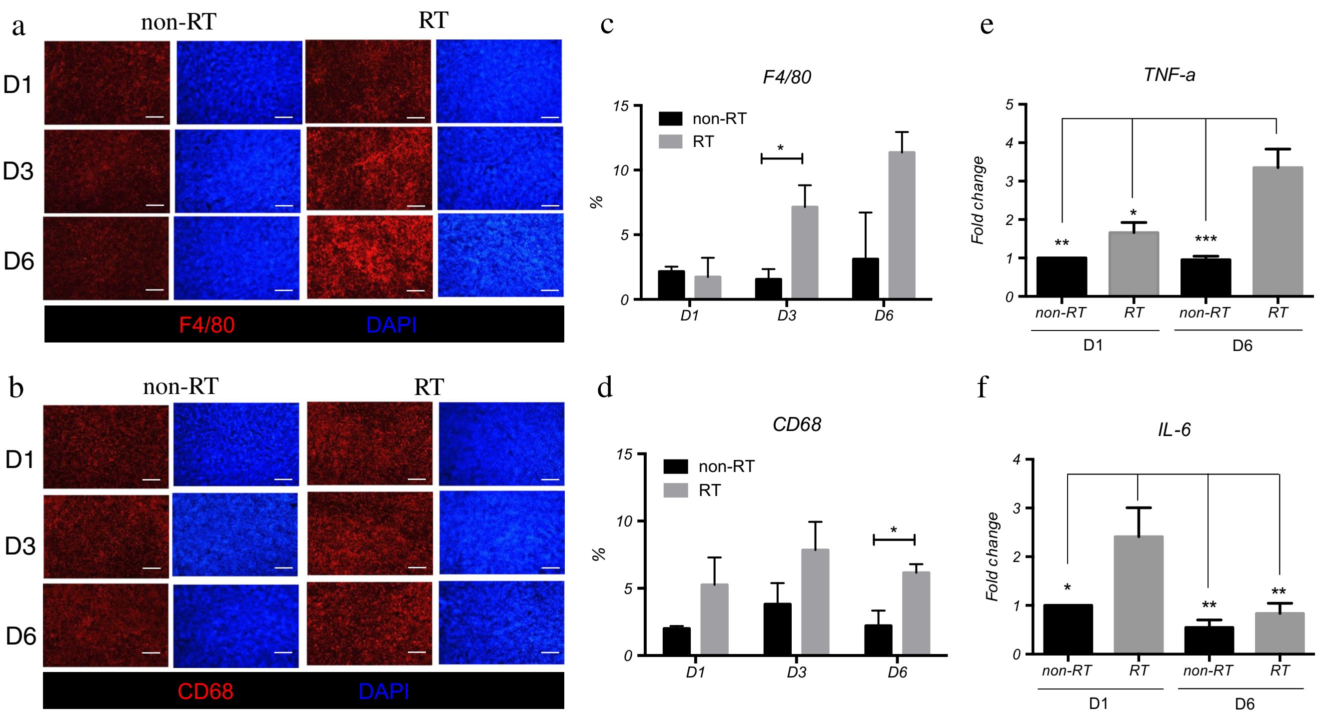

Fig. 5 Macrophage subpopulations within the tumor microenvironment identified using F4/80 and CD68 immunohistochemical staining. **a**, **b** Representative sections of HCC tumors stained with (**a**) F4/80 and DAPI and (**b**) CD68 and DAPI (×100, *scale bar* 50 μm). **c**, **d** Quantitative comparison of (**c**) F4/80-positive and (**d**) CD68-positive macrophage populations in non-RT and RT groups (three mice per group). At least eight fields were analyzed for each tumor (*$P < 0.05$). **e**, **f** Quantitative results of (**e**) TNF-α and (**f**) IL-6 expression by real-time PCR in non-RT and RT groups (three to seven mice per group; *$P < 0.05$, **$P < 0.01$, ***$P < 0.001$) *D1–D6* days 1–6

radiation caused an influx of macrophages into tumors and induced an early inflammatory response.

To determine whether tumor-infiltrating macrophages contributed to elevated glucose uptake in the RT group, an in vitro study was performed in which ^{18}F-FDG uptake was measured in macrophage (RAW) and HCC (BNL) cell lines. To identify the major contributor to ^{18}F-FDG uptake after irradiation, three culture conditions were tested: culture in separate dishes and in Transwell dishes (without cell–cell contact) and cocultures (with cell–cell contact). When RAW and BNL cells were cultured separately or in Transwell dishes, ^{18}F-FDG uptake in both cell types was lower in the RT group than in the non-RT group. However, in RAW–BNL cocultures, ^{18}F-FDG uptake at 3 h was significantly higher ($P < 0.05$) in the RT group than in the non-RT group, and the uptake then recovered to a level similar to that in the non-RT group at 24 h (Table 1). These

Table 1 ^{18}F-FDG uptake measured in BNL and RAW 264.7 cells cultured separately, in Transwell dishes and as cocultures at 3 and 24 h

Culture conditions		Non-RT	RT	*P* value
BNL				
Separate	3 h	0.023 ± 0.006	0.020 ± 0.006	–
	24 h	0.017 ± 0.002	0.015 ± 0.001	<0.05
Transwell	3 h	0.030 ± 0.01	0.010 ± 0.005	<0.001
	24 h	0.020 ± 0.007	0.007 ± 0.005	<0.01
RAW 264.7				
Separate	3 h	0.022 ± 0.009	0.021 ± 0.005	–
	24 h	0.032 ± 0.002	0.023 ± 0.004	<0.001
Transwell	3 h	0.010 ± 0.004	0.005 ± 0.004	<0.01
	24 h	0.040 ± 0.033	0.006 ± 0.004	–
BNL–RAW 264.7 coculture (5:1)	3 h	0.029 ± 0.006	0.040 ± 0.010	<0.05
	24 h	0.018 ± 0.006	0.019 ± 0.006	–

The values presented are counts per cell, mean ± standard deviation; initial BNL or RAW 264.7 cell seeding number 3×10^4

results suggest that contact between tumor cells and macrophages is required for glucose uptake to increase after irradiation.

Discussion

This study characterized the responses of HCC tumors in situ to radiation treatment using multi-imaging modalities, and validated the changes at the cellular level using IHC staining and in vitro culture systems. T2-weighted MRI revealed potent tumor control for 13 days after radiation treatment, and DW MRI showed that ADC values were significantly increased in the RT group as early as 1 day after irradiation ($P < 0.01$ vs. non-RT) and remained higher than in the non-RT group thereafter. Furthermore, a parallel study of tumor metabolism revealed an early increase in ^{18}F-FDG uptake on day 1, and this was sustained until 6 days after irradiation. Lastly, the results of IHC staining and real-time PCR indicated reduced cell proliferation, increased macrophage infiltration and induced inflammatory gene expression in radiation-treated tumors at all time-points examined.

ADC changes after irradiation

ADC values derived from DW MRI have been reported to correlate with cell density. Increases in cell density restrict water diffusion and decrease ADC values [16, 17]. However, previous clinical studies have shown a disparity in ADC values between different cancer types: the correlation between ADC values and tumor cellularity is good in glioma but poor in lymphoma [18, 19]. Zhao et al. found that ADC values increased in 10 days after sorafenib treatment of xenograft HCC tumors established in immunocompromised mice [20]. Here, we established the HCC tumor model in immunocompetent mice and found that irradiation with 15 Gy to tumor sites induced substantial increases in ADC values as early as 1 day after irradiation and that this increase was maintianed until the end of the observation period. One potential reason for the early changes in ADC is irradiation-induced apoptosis in tumors. The decrease in density of the tumor mass could lead to an increase in unrestricted water molecule diffusion. However, our IHC data did not support this hypothesis: apoptotic cells in tumors on day 1 were not more numerous in the RT group than in the non-RT group (data not shown). Tumor cells under radiation-induced stress might die through distinct mechanisms, such as autophagy or senescence, but we did not test this experimentally in this study.

As in previous studies, the necrotic/edematous areas showed high ADC values [21, 22] at diagnosis. The extent of tumor necrosis was assessed by HE staining. On day 1 after irradiation, similar necrotic area percentages were found in the non-RT and RT groups (about 18%). However, on day 6 after irradiation, the necrotic area increased to 40% in the non-RT group and remained at 18% in the RT group. Therefore, the increase in the area of necrosis was not correlated with the increase in ADC values in the RT group. Treated tumors usually showed a mixed histology including viable tumor cells, necrosis and granulation tissue. Thus, ADC values cannot be a specific predictor of biological changes. In our study, the increase in ADC values in HCC tumors after irradiation implies that radiation influences tumor cellularity mainly by decreasing proliferation rather than by inducing cell death from apoptosis or necrosis.

Another explanation for the changes in ADC values may be derived from the study by Zhang et al. who found that changes in ADC values are negatively correlated with the Ki67 proliferation index in the CT26 colorectal tumor model after radiotherapy [23]. Our data on Ki67-positive cells agree with this finding. The number of proliferating cells gradually decreased in the RT group, but increased in the non-RT group. Conversely, ADC values were higher in the RT group than in the non-RT group. These results suggest a negative correlation between ADC values and the Ki67 proliferation index in this tumor model. In addition to tumor death and reduced proliferation, continuous macrophage infiltration into the tumor mass occurred after irradiation. The influx of these immune cells, which were small and accounted for up to 18% of the total cell population in tumors, might be the main cause of the decrease in cell density in the RT group, which would lead to an increase in ADC values. The radiation-induced immune cell influx was not tumor- or tissue-dependent because similar findings have been obtained previously [24–26], and this suggests that the influx is a general response to irradiation. Our study revealed that DW MRI is a feasible method for estimating changes in ADC values after irradiation and their correlation with cell density, which indicates the potential of this measurement as a surrogate for predicting early tumor responses to treatment.

^{18}F-FDG uptake associated with immunity-inducing inflammation

The relevance of the inflammatory response to radiation treatment has been addressed previously [27–29]. Radiation induces cell death through apoptosis and/or necrosis by inducing the proinflammatory pathway primarily through activation of NF-κB, the main mediator of inflammation, carcinogenesis, and radioresistance [30, 31]. Immune cells such as macrophages and neutrophils are recruited in response to IL-6 release induced by NF-κB activation [32]. Given that radiation treatment is widely used, immune responses in relation to time in preclinical tumors receiving radiotherapy should be investigated, particularly using noninvasive molecular imaging. In the clinic, the use of ^{18}F-FDG PET for monitoring tumor responses to radiation therapy is limited by the false-positive signal resulting from the presence of inflammation, which hinders the application of the method during the 4–6 weeks after administration of the last fraction of radiation [33]. However, experimental findings remain debated because diverse radiation doses and in vitro/in vivo tumor models have been used. In an in vitro study, ^{18}F-FDG uptake in an ovarian cancer cell line (HTB77IP3) increased from day 0 to 12 after irradiation with 30 Gy relative to the uptake in nonirradiated cells [34]. Conversely, in a xenograft tumor model, irradiation with 6 Gy caused a decrease in ^{18}F-FDG uptake on day 1 [35]. The drawback of these studies is that a complete immune system was lacking and the contribution of the immune response to ^{18}F-FDG uptake was not considered.

In our study, an orthotopic HCC model was established in immunocompetent mice, and partial irradiation was administered only to the right liver lobe to spare the remaining liver tissue and avoid severe tissue inflammation. The increase in ^{18}F-FDG uptake from day 1 to day 6 after irradiation relative to baseline was not due to an increase in tumor cell number because the Ki67 index decreased, but was suspected to result from an inflammatory response. Moreover, IHC staining revealed marked increases in two macrophage populations, F4/80-positive and CD68-positive, 6 days after irradiation. This presence of macrophages in the tumor microenvironment contributed to the inflammatory response in the tumor from day 1 to day 6 after irradiation. Overall, the combination of an increase in macrophages and a decrease in the number of proliferative tumor cells led to a slight elevation in SUVmax in the RT group. We also measured cellular FDG uptake in vitro to integrate the findings with the in vivo imaging results. In BNL and RAW cells cultured in separate dishes or in Transwell dishes, ^{18}F-FDG uptake was lower in irradiated than in non-irradiated cells, which might have been due to cell cycle arrest caused by irradiation-induced stress. In contrast, ^{18}F-FDG uptake at 3 h after irradiation with 2 Gy was increased in RAW–BNL cocultures, which indicates that contact between macrophages and tumor cells is required to enhance glucose transport. Here, to evaluate the tumor response to irradiation using ^{18}F-FDG PET, the immune cell content and tumor cell death/proliferation must be carefully considered. Moreover, an extended observation period is necessary to monitor the dynamic profile of immune cell populations in the tumor microenvironment for interpreting ^{18}F-FDG PET results.

Limitations

In this study, the area exposed to the external radiation beam was not confirmed using an image-guided system. An irradiation field near (1 cm from) the right side of the xiphoid process was used, and this covered the right liver lobe and the tumor. Furthermore, the consciousness and movement of the animals during irradiation coiuld not be monitored. Therefore, the radiation dose might not have been successfully delivered to tumor sites in every mouse. Another limitation is that we did not use inflammation-associated PET tracers instead of ^{18}F-FDG to monitor the radiation response. Because ^{18}F-FDG is not a specific tracer for inflammation, the uptake measured in the tumor provides comprehensive information that includes inflammatory and tumor responses to radiation treatment. Several PET tracers are currently used in radiotherapy response assessment and radiation treatment planning. ^{18}F-Fluorocholine PET has demonstrated that changes in SUVmax during radiation treatment can predict clinical outcomes in several cancer types [36]. Moreover, in a study evaluating ^{18}F-fluorothymidine (FLT) PET/CT in patients with cervical and vaginal cancers, ^{18}F-FLT uptake was found to be markedly decreased after chemoradiotherapy, which suggests that inflammation exerts no notable effect on ^{18}F-FLT uptake [37]. The use of a new PET tracer, ^{89}Zr-oxalate, for monitoring inflammation has been investigated in mouse models of inflammation, tumor, and rheumatoid arthritis [38]. In this study, we investigated the use of ^{11}C-choline and ^{11}C-acetate for tumor imaging in our HCC mouse model, but accumulation of large amounts of radioactivity in the liver resulted in poor contrast images (Supplementary Fig. 1). Although ^{18}F-FDG, an extensively used PET tracer, might not be an inflammation-specific tracer for investigating the immune response to irradiation, selection of an appropriate measurement time-point could likely enable evaluation of the inflammatory effects in tumors.

Future direction

Radiation therapy has not played a prominent role in HCC treatment. However, in patients with inoperable HCC, advanced computer technology and sophisticated external-beam radiation treatment planning make radiation therapy a viable treatment option. Proton therapy, which produces fewer side effects in normal tissue and features a higher therapeutic ratio, is emerging as a promising treatment strategy in some HCC patients. In future studies, we intend to assess early tumor responses to proton therapy using multimodality non-invasive imaging in the preclinical setting and expect to be able to transfer this experience to clinical treatment.

Conclusion

DW MRI and ^{18}F-FDG PET multi-imaging can be used to evaluate the early response to radiation treatment in HCC. The increased ADC values derived from DW MRI could provide crucial evidence indicating tumor responses to radiation as early as on day 1 after irradiation. Moreover, radiation-induced immune cell influx was the predominant event among the changes in the tumor microenvironment in the first 6 days after irradiation, and ^{18}F-FDG uptake could be used effectively to evaluate the integration of tumor response and immune system activation in HCC mice 6 days after irradiation. Overall, exploitation of molecular functional imaging for early assessment of the effects of radiation yielded more promising results than did histological analysis for morphological assessment.

Acknowledgments We thank the Radiation Biology Core Laboratory, Chang Gung Memorial Hospital, for their support in performing the radiation treatments and in immunohistochemistry imaging, and the Center for Advanced Molecular Imaging and Translation, Chang Gung Memorial Hospital, for their support in imaging.

Funding This study was supported by Chang Gung Medical Foundation, Taiwan (grants CRRPG3E0014, CMRPG3B0313, and CMRPD1H0471) and the Ministry of Science and Technology (MOST 107-2314-B-182-068-MY2 to Fang-Hsin Chen, and MOST 106-2627-M-182A-002 to Tzu-Chen Yen).

Compliance with ethical standards

Conflicts of interest None.

Ethical approval All procedures used in animal studies were in accordance with the ethical standards of our institution.

References

1. Ippolito D, Fior D, Trattenero C, Ponti ED, Drago S, Guerra L, et al. Combined value of apparent diffusion coefficient-standardized uptake value max in evaluation of post-treated locally advanced rectal cancer. World J Radiol. 2015;7:509–20.
2. Zhu RX, Seto WK, Lai CL, Yuen MF. Epidemiology of hepatocellular carcinoma in the Asia-Pacific region. Gut Liver. 2016;10:332–9.
3. Reed GB Jr, Cox AJ Jr. The human liver after radiation injury. A form of veno-occlusive disease. Am J Pathol. 1966;48:597–611.
4. Kalogeridi MA, Zygogianni A, Kyrgias G, Kouvaris J, Chatziioannou S, Kelekis N, et al. Role of radiotherapy in the management of hepatocellular carcinoma: a systematic review. World J Hepatol. 2015;7:101–12.
5. Therasse P, Arbuck SG, Eisenhauer EA, Wanders J, Kaplan RS, Rubinstein L, et al. New guidelines to evaluate the response to treatment in solid tumors. European Organization for Research and Treatment of Cancer, National Cancer Institute of the United States, National Cancer Institute of Canada. J Natl Cancer Inst. 2000;92:205–16.
6. Oya N, Nagata Y, Tamaki N, Takagi T, Murata R, Magata Y, et al. FDG-PET evaluation of therapeutic effects on VX2 liver tumor. J Nucl Med. 1996;37:296–302.
7. Santos P, Peck KK, Arevalo-Perez J, Karimi S, Lis E, Yamada Y, et al. T1-weighted dynamic contrast-enhanced MR perfusion imaging characterizes tumor response to radiation therapy in chordoma. AJNR Am J Neuroradiol. 2017;38:2210–6.
8. Magne N, Toillon RA, Bottero V, Didelot C, Houtte PV, Gerard JP, et al. NF-kappaB modulation and ionizing radiation: mechanisms and future directions for cancer treatment. Cancer Lett. 2006;231:158–68.
9. Nair VS, Gevaert O, Davidzon G, Plevritis SK, West R. NF-kappaB protein expression associates with (18)F-FDG PET tumor uptake in non-small cell lung cancer: a radiogenomics validation study to understand tumor metabolism. Lung Cancer. 2014;83:189–96.
10. Purandare NC, Puranik AD, Shah S, Agrawal A, Rangarajan V. Post-treatment appearances, pitfalls, and patterns of failure in head and neck cancer on FDG PET/CT imaging. Indian J Nucl Med. 2014;29:151–7.
11. Sanuki N, Takeda A, Oku Y, Eriguchi T, Nishimura S, Aoki Y, et al. Threshold doses for focal liver reaction after stereotactic ablative body radiation therapy for small hepatocellular carcinoma depend on liver function: evaluation on magnetic resonance imaging with Gd-EOB-DTPA. Int J Radiat Oncol Biol Phys. 2014;88:306–11.
12. Liu HL, Hsu PH, Lin CY, Huang CW, Chai WY, Chu PC, et al. Focused ultrasound enhances central nervous system delivery of bevacizumab for malignant glioma treatment. Radiology. 2016;281:99–108.
13. Chen L, Liu M, Bao J, Xia Y, Zhang J, Zhang L, et al. The correlation between apparent diffusion coefficient and tumor cellularity in patients: a meta-analysis. PLoS One. 2013;8:e79008.
14. Shih YH, Peng CL, Chiang PF, Lin WJ, Luo TY, Shieh MJ. Therapeutic and scintigraphic applications of polymeric micelles: combination of chemotherapy and radiotherapy in hepatocellular carcinoma. Int J Nanomedicine. 2015;10:7443–54.
15. Chen FH, Wang CC, Liu HL, Fu SY, Yu CF, Chang C, et al. Decline of tumor vascular function as assessed by dynamic contrast-enhanced magnetic resonance imaging is associated with poor responses to radiation therapy and chemotherapy. Int J Radiat Oncol Biol Phys. 2016;95:1495–503.
16. Galons JP, Lope-Piedrafita S, Divijak JL, Corum C, Gillies RJ, Trouard TP. Uncovering of intracellular water in cultured cells. Magn Reson Med. 2005;54:79–86.
17. Harkins KD, Galons JP, Secomb TW, Trouard TP. Assessment of the effects of cellular tissue properties on ADC measurements by numerical simulation of water diffusion. Magn Reson Med. 2009;62:1414–22.
18. Surov A, Meyer HJ, Wienke A. Correlation between apparent diffusion coefficient (ADC) and cellularity is different in several tumors: a meta-analysis. Oncotarget. 2017;8:59492–9.
19. Yoshikawa MI, Ohsumi S, Sugata S, Kataoka M, Takashima S, Mochizuki T, et al. Relation between cancer cellularity and apparent diffusion coefficient values using diffusion-weighted magnetic resonance imaging in breast cancer. Radiat Med. 2008;26:222–6.
20. Zhao YL, Guo QQ, Yang GR, Wang QD. Early changes in apparent diffusion coefficient as an indicator of response to sorafenib in hepatocellular carcinoma. J Zhejiang Univ Sci B. 2014;15:713–9.
21. Gluskin JS, Chegai F, Monti S, Squillaci E, Mannelli L. Hepatocellular carcinoma and diffusion-weighted MRI: detection and evaluation of treatment response. J Cancer. 2016;7:1565–70.
22. Taouli B, Koh DM. Diffusion-weighted MR imaging of the liver. Radiology. 2010;254:47–66.
23. Zhang XY, Sun YS, Tang L, Xue WC, Zhang XP. Correlation of diffusion-weighted imaging data with apoptotic and proliferation indexes in CT26 colorectal tumor homografts in balb/c mouse. J Magn Reson Imaging. 2011;33:1171–6.
24. Tsai CS, Chen FH, Wang CC, Huang HL, Jung SM, Wu CJ, et al. Macrophages from irradiated tumors express higher levels of iNOS, arginase-I and COX-2, and promote tumor growth. Int J Radiat Oncol Biol Phys. 2007;68:499–507.
25. Rades D, Stalpers LJ, Veninga T, Hoskin PJ. Spinal reirradiation after short-course RT for metastatic spinal cord compression. Int J Radiat Oncol Biol Phys. 2005;63:872–5.
26. Chiang CS, Fu SY, Wang SC, Yu CF, Chen FH, Lin CM, et al. Irradiation promotes an m2 macrophage phenotype in tumor hypoxia. Front Oncol. 2012;2:89.
27. Di Maggio FM, Minafra L, Forte GI, Cammarata FP, Lio D, Messa C, et al. Portrait of inflammatory response to ionizing radiation treatment. J Inflamm (Lond). 2015;12:14.

28. Multhoff G, Radons J. Radiation, inflammation, and immune responses in cancer. Front Oncol. 2012;2:58.
29. Schaue D, Jahns J, Hildebrandt G, Trott KR. Radiation treatment of acute inflammation in mice. Int J Radiat Biol. 2005;81:657–67.
30. Kern P, Keilholz L, Forster C, Seegenschmiedt MH, Sauer R, Herrmann M. In vitro apoptosis in peripheral blood mononuclear cells induced by low-dose radiotherapy displays a discontinuous dose-dependence. Int J Radiat Biol. 1999;75:995–1003.
31. Deorukhkar A, Krishnan S. Targeting inflammatory pathways for tumor radiosensitization. Biochem Pharmacol. 2010;80:1904–14.
32. Rincon M. Interleukin-6: from an inflammatory marker to a target for inflammatory diseases. Trends Immunol. 2012;33:571–7.
33. Zhu A, Lee D, Shim H. Metabolic positron emission tomography imaging in cancer detection and therapy response. Semin Oncol. 2011;38:55–69.
34. Higashi K, Clavo AC, Wahl RL. In vitro assessment of 2-fluoro-2-deoxy-D-glucose, L-methionine and thymidine as agents to monitor the early response of a human adenocarcinoma cell line to radiotherapy. J Nucl Med. 1993;34:773–9.
35. Hu P, Cheng D, Huang T, Banizs AB, Xiao J, Liu G, et al. Evaluation of novel (64)Cu-labeled theranostic gadolinium-based Nanoprobes in HepG2 tumor-bearing nude mice. Nanoscale Res Lett. 2017;12:523.
36. Parashar B, Wernicke AG, Rice S, Osborne J, Singh P, Nori D, et al. Early assessment of radiation response using a novel functional imaging modality – [18F]fluorocholine PET (FCH-PET): a pilot study. Discov Med. 2012;14:13–20.
37. Cho LP, Kim CK, Viswanathan AN. Pilot study assessing (18)F-fluorothymidine PET/CT in cervical and vaginal cancers before and after external beam radiation. Gynecol Oncol Rep. 2015;14:34–7.
38. Park JA, Lee YJ, Lee JW, Yoo RJ, Shin UC, Lee KC, et al. Evaluation of [(89)Zr]-oxalate as a PET tracer in inflammation, tumor, and rheumatoid arthritis models. Mol Pharm. 2016;13:2571–7.